Loss of nucleus accumbens low-frequency fluctuations is a signature of chronic pain

Meena M. Makary[a,b,c,d], Pablo Polosecki[e], Guillermo A. Cecchi[e], Ivan E. DeAraujo[f], Daniel S. Barron[b], Todd R. Constable[g], Peter G. Whang[h], Donna A. Thomas[i], Hani Mowafi[j], Dana M. Small[b], and Paul Geha[a,b,k,1]

[a]The John B. Pierce Laboratory, New Haven, CT 06519; [b]Department of Psychiatry, Yale School of Medicine, Yale University, New Haven, CT 06511; [c]Athinoula A. Martinos Center for Biomedical Imaging, Department of Radiology, Massachusetts General Hospital, Harvard Medical School, Charlestown, MA 02129; [d]Systems and Biomedical Engineering Department, Faculty of Engineering, Cairo University, 12613 Giza, Egypt; [e]Health Care and Life Sciences, IBM Research, Thomas J. Watson Research Center, Yorktown Heights, NY 10598; [f]Department of Neuroscience, Icahn School of Medicine at Mount Sinai, New York, NY 10029; [g]Computational Radiology and Biomedical Imaging, Yale School of Medicine, Yale University, New Haven, CT 06520; [h]Department of Orthopaedics and Rehabilitation, Yale School of Medicine, Yale University, New Haven, CT 06510; [i]Department of Anesthesiology, Yale School of Medicine, Yale University, New Haven, CT 06520; [j]Yale Emergency Medicine, Yale School of Medicine, Yale University, New Haven, CT 06519; and [k]Department of Psychiatry, School of Medicine and Dentistry, University of Rochester, Rochester, NY 14642

Edited by Peter L. Strick, University of Pittsburgh, Pittsburgh, PA, and approved March 10, 2020 (received for review October 28, 2019)

Chronic pain is a highly prevalent disease with poorly understood pathophysiology. In particular, the brain mechanisms mediating the transition from acute to chronic pain remain largely unknown. Here, we identify a subcortical signature of back pain. Specifically, subacute back pain patients who are at risk for developing chronic pain exhibit a smaller nucleus accumbens volume, which persists in the chronic phase, compared to healthy controls. The smaller accumbens volume was also observed in a separate cohort of chronic low-back pain patients and was associated with dynamic changes in functional connectivity. At baseline, subacute back pain patients showed altered local nucleus accumbens connectivity between putative shell and core, irrespective of the risk of transition to chronic pain. At follow-up, connectivity changes were observed between nucleus accumbens and rostral anterior cingulate cortex in the patients with persistent pain. Analysis of the power spectral density of nucleus accumbens resting-state activity in the subacute and chronic back pain patients revealed loss of power in the slow-5 frequency band (0.01 to 0.027 Hz) which developed only in the chronic phase of pain. This loss of power was reproducible across two cohorts of chronic low-back pain patients obtained from different sites and accurately classified chronic low-back pain patients in two additional independent datasets. Our results provide evidence that lower nucleus accumbens volume confers risk for developing chronic pain and altered nucleus accumbens activity is a signature of the state of chronic pain.

chronic pain | limbic system | nucleus accumbens | magnetic resonance imaging

Chronic pain is a huge burden to individuals and society. It decreases quality of life leading sometimes to disability (1), predisposes patients to other comorbidities such as substance misuse, and causes billions of dollars in economic losses every year (2). The pathophysiology of chronic pain in humans has been subject to intensive investigation with functional brain imaging in the past two decades in the hope of identifying brain circuits that underlie the risk and the subjective experience of chronic pain. This endeavor is critical to uncovering biomarkers of this condition that could inform diagnosis, prevention, and novel treatments (3).

Two recent functional MRI (fMRI) studies suggest that the risk of transitioning from acute to chronic pain may be determined by the physiology of the limbic brain (4, 5). In addition, preclinical studies have provided evidence that the limbic brain plays a causal role in the modulation of peripheral nociception (6–8) and in the transition to chronic pain (7, 9). However, a state-specific biomarker for chronic pain is still unknown and a robust reproducible biomarker remains undefined.

In the present study we examined the structural and functional properties of limbic structures (amygdala, accumbens, hippocampus, and thalamus) in healthy participants, in patients suffering from subacute back pain (SBP), and in patients suffering from chronic low-back pain (CLBP). After initial testing, we also followed the SBP patients and healthy participants longitudinally and identified patients who persist in having pain (SBPp) and patients who recover (SBPr). Specifically, we measured subcortical brain volumes and resting-state brain activity. These analyses revealed two findings pertaining to the role of the brain in risk and development of chronic pain. First, a smaller nucleus accumbens volume predates the development of chronic pain and remains unchanged at follow-up, suggesting that it plays a role in risk for development of chronic pain. Second, alterations in low-frequency (0.01 to 0.027 Hz) oscillations at rest in the nucleus accumbens develop only after the onset of the chronic pain phase, suggesting that it is a signature of the state of chronic pain.

Significance

The prevalence of chronic pain has reached epidemic levels. In addition to personal suffering, chronic pain is associated with psychiatric and medical comorbidities, notably substance misuse. Chronic pain does not have a cure or quantitative diagnostic or prognostic tools. Here we show that brain imaging can provide such measures. First, we show that the brain limbic system of patients with subacute back pain at risk for becoming chronic back pain patients exhibits limbic system structural alterations, which predate the onset of chronic pain. Second, we show that the nucleus accumbens activity shows loss of low-frequency fluctuations only when patients transition to the chronic phase, an observation that was reproduced in multiple datasets collected at different sites.

Author contributions: I.E.D., D.M.S., and P.G. designed research; M.M.M., P.G.W., D.A.T., H.M., D.M.S., and P.G. performed research; M.M.M., P.P., G.A.C., D.S.B., T.R.C., D.M.S., and P.G. analyzed data; M.M.M., P.P., G.A.C., D.M.S., and P.G. wrote the paper; and I.E.D. provided advice during data analysis.

The authors declare no competing interest.

This article is a PNAS Direct Submission.

Data deposition: Demographic, clinical, and brain imaging data at baseline and at follow-up have been deposited in the OpenPain repository, ftp://openpain.org/AccumbensChronicPainSignature.

[1]To whom correspondence may be addressed. Email: paul_geha@urmc.rochester.edu.

This article contains supporting information online at https://www.pnas.org/lookup/suppl/doi:10.1073/pnas.1918682117/-/DCSupplemental.

First published April 20, 2020.

Results

The Volume of the Nucleus Accumbens Is Smaller in Subacute and Chronic Low-Back Pain Patients. The left nucleus accumbens (LNAc) showed a significant decrease in volume when healthy participants were compared to SBP and CLBP patients [$F_{(2,93)}$ = 6.0; $P = 0.004$; Cohen's $d = 0.70$] (healthy volume = 0.76 ± 0.02; SBP volume = 0.69 ± 0.02; CLBP = 0.66 ± 0.02 cc) (Fig. 1*A* and *SI Appendix*, Table S2). Post hoc Tukey's honestly significant difference (HSD) showed that the LNAc was significantly smaller in SBP ($P = 0.034$) and CLBP patients ($P = 0.003$) compared to healthy participants. There was no group effect in the right NAc (RNAc) ($P = 0.20$). We did not find any difference in the hippocampus or amygdala volumes between healthy participants and back-pain patients (*SI Appendix*, Fig. S2). We repeated the volumetric analysis using FreeSurfer (10). The general linear model (GLM) analysis for LNAc ($P = 0.15$) and RNAc ($P = 0.21$) were not significant but post hoc HSD showed that CLBP patients show significantly smaller LNAc ($P = 0.02$) and RNAc ($P = 0.036$) than SBP patients (*SI Appendix*, Fig. S3). We examined the correlations between the volumetric values obtained with FIRST and those obtained with FreeSurfer. The two protocols give weakly correlated results in smaller structures (i.e., NAc and amygdala) and strongly correlated results in larger structures (i.e., hippocampus and thalamus) (*SI Appendix*, Fig. S4), similar to a previous report (5). This explains in large part the discrepancy observed in the NAc volume obtained from the two subcortical extraction protocols. Signal-to-noise ratio (SNR) was not different for any subcortical structure when comparing healthy controls (HCs), SBP, and CLBP participants (*SI Appendix*, Fig. S5).

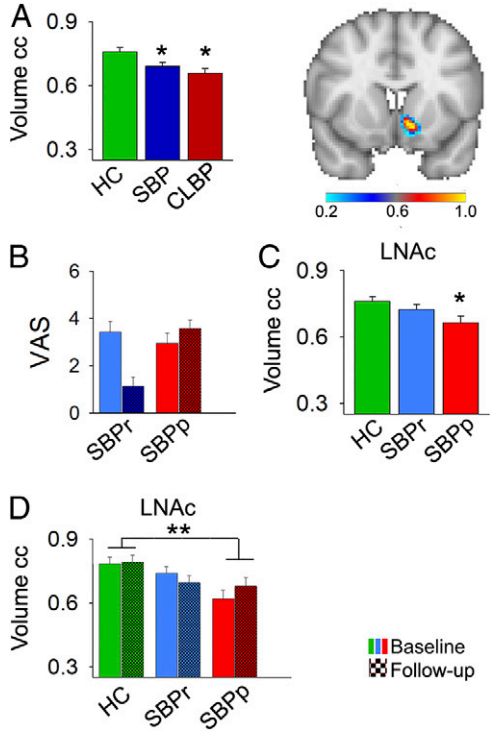

Fig. 1. Nucleus accumbens volume shrinks in back pain. (*A*) Left nucleus accumbens volume shows a gradual and significant decrease when comparing SBP and CLBP patients to healthy controls (GLM corrected for age and sex, $P < 0.01$). Brain slice on the *Right* shows heat map of overlap (from 0 to 1) in the automated segmentation of LNAc across CLBP and SBP patients and healthy controls at baseline. Brain orientation follows the radiological convention. (*B*) Back-pain intensity reported by SBP patients on a VAS scale drops significantly in SBPr patients but not in SBPp patients. (*C*) Left nucleus accumbens volume is already significantly smaller in SBPp patients at risk for transitioning to CLBP compared to healthy controls at entry into the study and (*D*) remains unchanged at follow-up (~1 y later). Checkered barplots show the average at follow-up. $^{**}P < 0.01$; $^{*}P < 0.05$, post hoc HSD compared to healthy controls.

NAc Volume Is Smaller in SBP Patients with Persistent Pain at Follow-Up. Thirty-five SBP patients and 16 healthy controls were followed after a median of 59.5 wk; 19 patients reported ≥30% improvement in their back-pain intensity and were considered recovered (SBPr) and 16 patients reported persistent back pain (SBPp) (Fig. 1*B*). Average duration of follow-up varied between groups because of outliers (*SI Appendix*, Fig. S1). Some participants were only available after more than 2 y of the initial baseline visit (*SI Appendix*, Fig. S1 and Table S3). At entry into the study, SBPp and SBPr patients did not differ on reported back-pain intensity (SBPp, 3.0 ± 0.4; SBPr = 3.5 ± 0.4, $P = 0.36$, unpaired t test) or the duration of back pain (SBPp, 9.9 ± 0.9; SBPr, 9.1 ± 0.9 wk, $P = 0.55$) (*SI Appendix*, Table S3); however, SBPr patients showed significantly higher Beck's Depression Inventory (BDI) ($P < 10^{-3}$, ANOVA) and Beck's Anxiety Inventory (BAI) ($P < 0.05$) scores than SBPp and healthy controls at baseline. Nevertheless, the BDI and BAI scores of SBPr patients fell within the mild depressive and mild anxiety range (*SI Appendix*, Table S3). SBPr patients showed significant improvement in their pain scores at follow-up, measured using the visual analog scale (VAS), the short form of McGill Pain Questionnaire (sfMPQ), the Neuropathic Pain Scale (NPS), and the Pain Catastrophizing Scale (PCS), and significant improvement in their mood but not their anxiety scores, while SBPp patients ratings did not show any change at follow-up (*SI Appendix*, Fig. S6*A* and Table S3). To investigate whether the decreased LNAc volume is present in SBPp patients at risk for transitioning to CLBP, we compared subcortical volumes of healthy controls ($n = 30$), SBPp ($n = 16$) and SBPr ($n = 19$) patients. At baseline, the volume of LNAc in SBPp patients was significantly smaller than the LNAc volume of healthy controls (and comparable to that in CLBP patients) [$F_{(2,59)}$ = 3.69; $P < 0.05$; Cohen's $d = 0.70$] (Fig. 1*C*). Post hoc comparison showed that SBPp patients had significantly ($P = 0.017$) smaller LNAc volume compared to healthy controls. A subset (26 SBP patients and 14 HCs) of these participants underwent also another fMRI scanning session at follow-up. Examining the volume of LNAc at follow-up showed persistence in the pattern observed at baseline where SBPp patients ($n = 11$) showed a significantly smaller LNAc compared to healthy controls ($n = 14$) and SBPr ($n = 15$) [GLM with repeated measures, $F_{(2,34)} = 5.1$; $P = 0.012$; Cohen's $d = 1.1$] (Fig. 1*D* and see also *SI Appendix*, Table S4). There was no change in the volume of LNAc between the two time points ($P = 0.40$). Since duration at follow-up varied between groups, we repeated the GLM analysis after adding duration at follow-up as a variable of no interest. The results remained unchanged with groups showing significant difference [$F_{(2,33)} = 4.8$; $P = 0.015$]. This is expected, given that LNAc volume does not significantly change over time. We did not observe any differences in the RNAc between SBPp, SBPr, and HC subjects (*SI Appendix*, Fig. S6*B*). NAc volume was not correlated to demographic parameters or measures of pain, anxiety, or depression (*SI Appendix*, Table S5). We did not observe significant differences in the volumes of amygdala or hippocampus in SBPp patients compared to SBPr patients or healthy controls at any visit of the study while using a repeated measures group × time analysis (*SI Appendix*, Fig. S6 and Table S4). However, examining baseline and follow-up volumes separately shows that SBPp patients have a significantly smaller amygdala volume than SBPr patients (adding left and right) at baseline as reported previously (5), but not at follow-up (*SI Appendix*, Fig. S7). SNR was not different for any subcortical structure when comparing healthy controls, SBPr, and SBPp participants (*SI Appendix*, Fig.

S8). The longitudinal results suggest that the volume of NAc is altered in SBPp patients by 6 to 16 wk after the onset of back pain and remains unchanged at long-term follow-up. Since previous reports (4, 5) used 20% drop in back-pain intensity at follow-up as a criterion defining recovery, we repeated the volumetric analysis after defining SBPr patients as such if their pain dropped by 20%. As a result, three SBP patients whose reduction in pain intensity fell between 20 and 30% were now considered recovered. *SI Appendix*, Fig. S9 shows that the volumetric results in the LNAc are almost identical. Next we asked whether decreased LNAc volume in SBPp patients is reproducible across different sites in patients made accessible through http://www.openpain.org/. Therefore, using an identical analysis to the one applied to our data in Fig. 1, we compared subcortical volumes from SBPp ($n = 32$; 26 at 1 y follow-up) and SBPr ($n = 22$; 17 at 1 y follow-up) patients and HC ($n = 18$; 17 at 1 y follow-up) groups using a within-subject repeated measures ANCOVA that accounts for age, sex, and intracranial volume. While we found a significantly smaller LNAc volume ($P = 0.03$, post hoc comparison to HCs) and a trend ($P = 0.06$) toward significance in the right NAc volume of SBPp patients at baseline, we did not observe a significant volumetric difference between the groups at follow-up (*SI Appendix*, Fig. S10*A*). However, when studying SNR, we observed that the data available online have a significantly smaller SNR than our data at all time points ($P < 10^{-6}$) (*SI Appendix*, Fig. S10*B*). The lower SNR can explain, at least in part, the discrepancy between sites, given the NAc's small size.

SBPp and SBPr Show Differences in Corticostriatal Functional Connectivity of Putative NAc Shell and Core. Next we asked whether the significant change in the volume of NAc in low-back pain patients is accompanied by functional connectivity (*fc*) changes. Given the well-known structural and functional differences between the nucleus accumbens shell and core demonstrated in animal studies (11, 12) and the recent evidence for the specific role of the NAc shell in acute and chronic pain animal models (7, 13–15) we studied the functional connectivity of the left and right NAc separately for putative shell and core based on recent parcellations reported using human fMRI (16, 17) (Fig. 2, *Inset*). *SI Appendix*, Fig. S11 shows the average seed *fc* of the putative NAc shell and core for CLBP patients and healthy controls. We first compared CLBP ($n = 27$) patients and healthy controls ($n = 30$) using ANCOVA corrected for age and sex. No significant differences were identified. Head motion parameters, estimated using absolute displacement and relative displacement, were not different between CLBP patients and healthy controls (*SI Appendix*, Fig. S12). Next we asked whether corticostriatal connectivity was different in SBPp and SBPr patients compared to healthy controls at baseline (16 SBPp and 19 SBPr patients, and 30 healthy controls) and/or at follow-up (11 SBPp and 14 SBPr patients, and 14 healthy controls) using ANCOVA. At baseline, ANCOVA analysis (i.e., *F* test) revealed decreased *fc* of putative LNAc shell in SBPp and SBPr patients compared to healthy controls within the limbic system. As such, SBPp patients showed decreased *fc* of putative LNAc shell to left thalamus, right and left NAc, right caudate, and rostral anterior cingulate cortex (rACC) (*SI Appendix*, Fig. S13) ($P < 0.05$, whole brain corrected). SBPr patients showed decreased *fc* of putative LNAc shell to left and right NAc and posterior ventral striatum (pallidum), right thalamus, and hypothalamus (*SI Appendix*, Fig. S13). No significant difference in *fc* was observed at follow-up between the three groups. Head motion parameters were not different between healthy controls, SBPp, and SBPr at baseline or at follow-up (*SI Appendix*, Fig. S12). Given the different functions of the NAc shell and core (12, 18) we next asked whether the differences in the *fc* of the two NAc subcircuitries are different among the groups. In a first step, the difference in *fc* between putative shell and core was calculated within each subject using Steiger's approach for "correlated correlations" (19). Hence, for a voxel X, putative shell and X (*r_sx*), and putative core and X (*r_cx*) correlations were calculated. Next, Steiger's *Z* value of the difference between *r_sx* and *r_cx*, which we designate as *δ-fc-NAc*, was derived. The resulting difference *Z* maps were finally entered into an ANCOVA analysis using nonparametric permutations. Using this approach, we did not observe any significant difference between CLBP patients and healthy controls. We however reasoned that dynamic changes in NAc shell and core connectivity could be occurring in SBP patients at baseline and as they transition to recovery or chronic pain. Therefore, we compared SBPp, SBPr, and healthy controls at both visits. At baseline, SBPp, SBPr, and healthy controls differed (*F* test, $P < 0.05$ corrected) in the LNAc (Fig. 2*A*), and post hoc analysis showed altered local NAc connectivity in SBP patients compared to controls. Healthy controls showed increased *δ-fc-NAc* in a cluster falling within the putative NAc shell compared to SBPr and to SBPp patients; SBP patients, on the other hand, showed an increased *δ-fc-NAc* in a cluster falling within the putative NAc core irrespective of long-term risk of transition to chronic pain (Fig. 2 *B* and *C*). At follow-up, ANCOVA analysis was close to significance ($P = 0.17$) within the rACC and post hoc analysis showed increased left *δ-fc-NAc* in the rACC in the SBPp patients compared to SBPr ($P < 0.05$, whole brain corrected) (Fig. 2*D*). The connectivity difference within the rACC was directly correlated to low-back intensity at follow-up across SBPp and SBPr patients ($r = 0.58$, $P < 0.01$) (Fig. 2*D*, scatterplot). Next, to investigate whether these group differences observed at each time point are significantly changing over time, we tested for effects of time using a within-subjects (11 SBPp and 14 SBPr patients, and 14 healthy controls) repeated measures design corrected for age and sex. In a first step, the left *δ-fc-NAc* maps within each subject were registered to a subject-specific template derived from the two anatomical images obtained at each time point, and the template was in turn registered to Montreal Neurologic Institute (MNI) space. The within-subject difference in time was tested against 10,000 permutations in a second step after accounting for age and sex. As such, the increased left *δ-fc-NAc* within the putative NAc core and the decreased left *δ-fc-NAc* within the putative shell in SBP patients compared to healthy controls observed at baseline (Fig. 2 *A–C*) is significantly changing (decreasing) in time (baseline > follow-up within subject analysis, $P < 0.05$ corrected; see *SI Appendix*, Fig. S14 *A–C*). The change in time for HC compared to SBPp patients did not reach significance ($P = 0.16$). However, the effects of time on the left *δ-fc-NAc* within the rACC observed at follow-up between SBPp and SBPr patients (Fig. 2*D*) is not significantly increased at follow-up compared to baseline. Here we also wanted to test whether the connectivity results presented in Fig. 2 were affected by our definition of recovery. Therefore, the analysis was repeated based on the 20% criterion for recovery. *SI Appendix*, Fig. S15*A* shows that, as expected, at baseline, the altered left *δ-fc-NAc* in SBP patients is independent of risk status. In addition, the increased left *δ-fc-NAc* connectivity in the rACC at follow-up in SBPp compared to SBPr patients remains significant. Here we also identified resting-state data available online from the Chicago study follow-up visit only in 10 SBPr, 20 SBPp patients, and 19 HCs and tested whether the altered left *δ-fc-NAc* we observed at follow-up can be identified across sites. Comparison between the three groups using ANCOVA did not yield any significant differences when testing left or right hemispheres.

Spectral Analysis. The results of the connectivity analysis uncovered differential changes in NAc putative shell and core *fc* between SBPp, SBPr patients, and healthy controls but did not identify a common brain biomarker between SBPp and CLBP

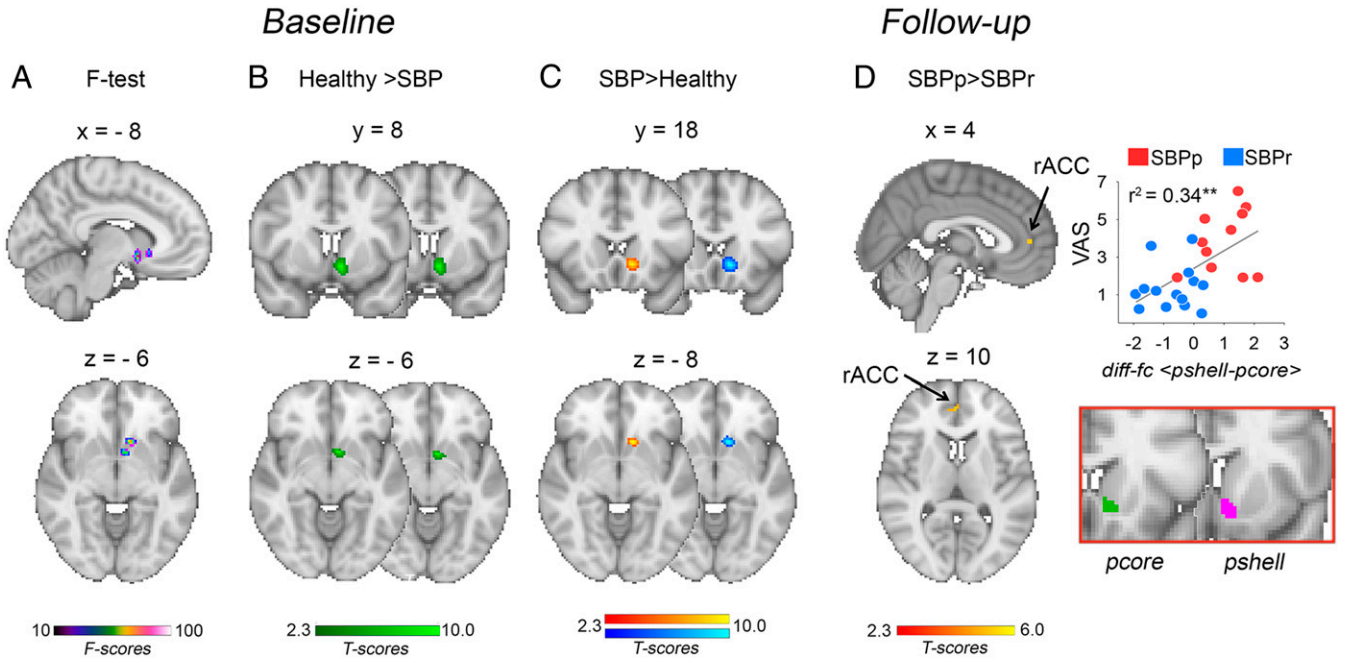

Fig. 2. The functional connectivity of the nucleus accumbens subcircuitry is altered in back pain. GLM results for the difference in functional connectivity between left nucleus accumbens putative shell and core at baseline (*A*–*C*) and at follow-up (*D*). (*A*) Differences in functional connectivity across all groups (SBPr, SBPp, and healthy controls) (*F* test) involves local NAc subcircuitries. (*B*) Healthy controls show increased difference in functional connectivity (*δ-fc-NAc*) between putative shell and core at baseline in the putative shell compared to both SBPp (slices to the *Left*) and SBPr (slices to the *Right*) patients. (*C*) SBP patients show increased difference in functional connectivity between putative shell and core at baseline in the putative core (*T* test). The contrast between SBPp patients and healthy controls is shown in red to yellow; the contrast between SBPr patients and healthy controls is shown in blue to light blue. (*D*) SBPp patients show increased difference in functional connectivity between putative shell and core within the rACC at follow-up. The scatterplot depicts the positive correlation between the rACC *δ-fc-NAc* values and back-pain intensity scores at follow-up (i.e., chronic phase) across SBPp and SBPr patients. *Inset* is a graphical depiction of putative shell (green) and core (violet) masks of nucleus accumbens based on ref. 16. Numbers on top of the brain slices indicate MNI coordinates in millimeters; results are presented after whole brain correction at $P < 0.05$; $^{**}P < 0.01$. Brain orientation follows the radiological convention.

patients that represents the "state" of being in chronic back pain. Functional connectivity results suggest that, as pain becomes chronic (i.e., >1 y), the NAc subcircuitries *fc* show dynamic changes. We therefore studied power spectral density (PSD) (20, 21) because this approach uncovered meaningful differences among clinical populations (22) including chronic pain patients (23–29). We calculated PSD for different frequency bands defined in previous neurophysiological and fMRI studies (21, 30, 31) in bilateral NAc and compared among groups using a hypothesis-based approach. We wanted to examine whether altered brain activity oscillations at specific frequency bands may characterize the chronic pain phase. First, we compared PSD between CLBP patients and healthy controls using an unpaired *t* test and a bilateral NAc mask. Comparison of PSD within the slow-5 frequency band (0.01 to 0.027 Hz) only showed significant differences between patients and control (Fig. 3 *A* and *B*). CLBP patients showed decreased power for low-frequency oscillations in a cluster falling within bilateral putative NAc core and shell ($P < 0.05$, region of interest [ROI] corrected). Next, we compared SBPp and SBPr patients and healthy controls at entry into the study and at follow-up using ANCOVA confined to bilateral NAc. This analysis revealed loss of power in the LNAc within the slow-5 frequency band in SBPp patients compared to SBPr patients at follow-up when pain became chronic ($P < 0.05$, ROI corrected) (Fig. 3 *C* and *D*). The cluster obtained falls within the putative NAc shell. In addition, PSD for the slow-5 band was inversely correlated to reported low-back pain intensity across both SBPp and SBPr patients ($r = -0.56$, $P < 0.01$) (Fig. 3*D*). We also tested whether using a 20% back-pain intensity decrease as a recovery criterion would affect the difference in slow-5 PSD within NAc between groups at follow-up. Using a similar analysis, we found that SBPp patients show a significant loss in slow-5 PSD compared to healthy controls within the left NAc but are no longer significantly different from SBPr patients ($P = 0.21$) (*SI Appendix*, Fig. S16). Since both PSD of the slow-5 frequency band and the difference between putative shell and core *fc* to rACC were significantly correlated to back-pain intensity at follow-up, we asked whether PSD and *δ-fc-NAc* relate independently to pain intensity. Partial correlations analysis of back-pain intensity with both variables (i.e., after removing the variance explained by the other) was significant for both PSD of slow-5 frequency band ($r = -0.43$, $P < 0.05$) and *fc* difference between putative shell and core within rACC ($r = 0.46$, $P < 0.05$). Next we asked whether this loss of power in slow-5 frequency band is reproducible in CLBP patients studied at different sites and made accessible through http://www.openpain.org/. Applying an identical analytic approach and pooling data collected in Chicago and Cambridge (Fig. 3*E*), we also observed loss of PSD within the slow-5 frequency band in RNAc in CLBP patients compared to healthy controls ($P < 0.05$, ROI corrected), despite the significant demographic and clinical heterogeneity of the CLBP patients' samples analyzed (*SI Appendix*, Fig. S17). If the loss of PSD within the slow-5 frequency band was directly related to the loss of volume in the NAc, we would have also observed loss of PSD within the other frequency bands (i.e., slow-2, -3, and -4). In addition, the loss of PSD within the slow-5 frequency band would have been apparent within the SBPp patients at baseline because these subjects do show a significantly smaller NAc at entry into the study. Nevertheless, we ran a multiple regression using our CLBP patients and healthy controls PSD data within

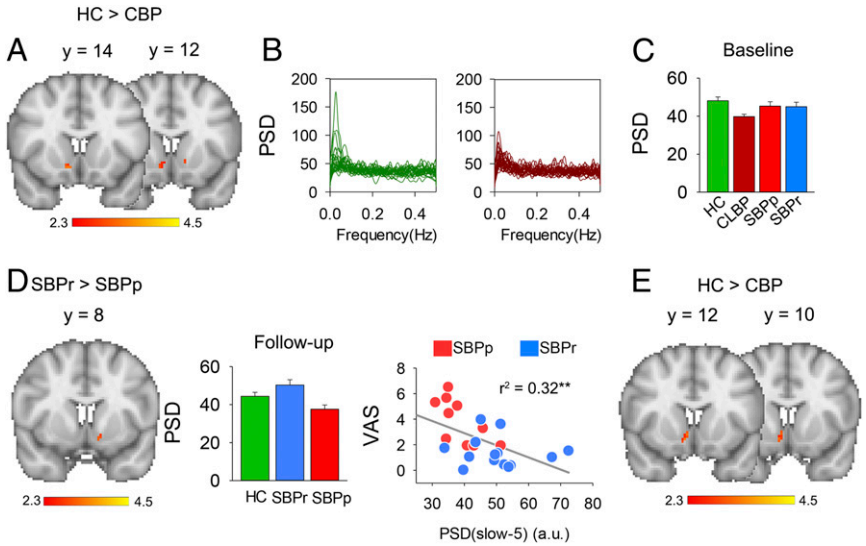

Fig. 3. Back-pain patients exhibit loss of power in the NAc within the slow-5 frequency band (0.01 to 0.027) as pain becomes chronic. (*A*) CLBP patients show decreased power within the slow-5 frequency band in bilateral NAc compared to healthy controls (unpaired *T* test, $P < 0.05$, ROI corrected). (*B*) Spectral plots as a function of frequency for healthy controls (green) and CLBP patients (dark red). (*C*) Illustration of average PSD within the NAc (summed over the cluster in *A* in healthy controls and CLBP patients); SBPp (bright red) and SBPr (light blue) PSD at baseline is not different from PSD in healthy controls over the same voxels depicted in *A*. (*D*) The same pattern observed in CLBP patients PSD is also seen in SBPp patients at follow-up when pain is chronic within left NAc illustrated in the histogram plot on the *Right*. This cluster falls within the left putative NAc shell. The PSD values of slow-5 frequency are inversely correlated to low-back pain intensity across both SBPr and SBPp patients. a.u., arbitrary units. (*E*) The pattern of loss of PSD within the slow-5 frequency band can also be observed in CLBP patients pooled from two different sites ($P < 0.05$, ROI corrected). $^{**}P < 0.05$.

bilateral NAc as a dependent variable and age, sex, group (CLBP vs. HC) and NAc volume as independent variables. Group remains a significant predictor of slow-5 PSD [mean PSD ± SEM for HC = 47.0 ± 1.6 and for CLBP patients = 39.8 ± 1.6; $\beta = 3.63$; $F_{(1,46)} = 9.0$, $P = 0.0043$]. The NAc volume did not significantly predict PSD ($\beta = 0.0082$; $P = 0.15$). Similar multiple regression was run on the SBPp, SBPr, and HC PSD data at follow-up. Group remains a significant predictor of slow-5 PSD [$\beta = 5.81$; $F_{(2,34)} = 6.4$; $P = 0.0042$], whereas LNAc volume is not ($P = 0.81$).

NAc Volume and Slow-5 PSD Can Accurately Classify Chronic Low Back Pain Patients. The volumetric and PSD results suggest that these features are potential predictors of being in chronic pain. Given that the slow-5 PSD in the nucleus accumbens showed the most robust reproducibility across studies and sites, we first tested the discriminative power of slow-5 PSD within the left and right NAc separately in classifying new data from the Chicago longitudinal study available from their follow-up visit (visit 4), using a simple cutoff (32) for evaluation of the areas under the receiver operating characteristic (ROC) curve (AUC). Slow-5 PSD extracted from the LNAc accurately classified 10 SBPr and 20 SBPp patients with an AUC = 0.75 ($P < 0.05$) (Fig. 4*A*), and 14 CLBP patients and 19 HC with an AUC = 0.73 ($P < 0.05$) (Fig. 4*B*). The PSD values in CLBP and HC were corrected for age (*SI Appendix*, Table S6). Next, we wanted to add the volume of the nucleus accumbens as a feature in a linear model to classify chronic back-pain patients. Therefore, we trained a linear support vector machine (SVM) model on data pooled from this study and the Cambridge data (45 CLBP patients and 65 HC subjects) using NAc slow-5 PSD and volume for each hemisphere separately. Next, using the model weights, we classified the 10 SBPr vs. 20 SBPp patients. Features extracted from the LNAc accurately classified SBPr and SBPp patients with AUC = 0.72 ($P < 0.05$). (Fig. 4*C*). We also tested our model on the 14 CLBP patients and 19 HC subjects available from the same follow-up visit, part of the Chicago longitudinal data. The prediction in this case did not reach significance (AUC = 0.61, $P = 0.15$). The results presented in Fig. 4 *A*–*D*, respectively, use the same test dataset; hence, the test dataset was used twice in our analysis.

Discussion

Patients suffering from low-back pain showed smaller NAc volume that predated the transition to the chronic phase and loss of PSD within the slow-5 (0.01 to 0.027 Hz) frequency band that developed as pain became chronic. The loss of PSD is a robust finding that was reproduced across samples and across sites and accurately classified chronic low-back pain patients from an independent dataset. In addition, NAc subcircuitries exhibited dynamic changes in functional connectivity as low-back pain patients transitioned from the subacute to the chronic phase. Altered local NAc differential connectivity between putative NAc shell and core was associated with the subacute phase irrespective of risk of "chronification," whereas increased differential connectivity between putative shell and core to the rACC was associated with the chronic phase and covaried directly with reported back-pain intensity. Time effects analysis confirmed the early involvement of the NAc subcircuitry during the subacute phase; however, the increased differential connectivity of the left NAc to the rACC did not significantly change in time and hence remains to be confirmed in future studies. In addition to the NAc, the amygdala volume at baseline was smaller in SBPp compared to SBPr patients and accurately classified patients by long-term risk for CLBP. Our findings agree with preclinical data showing a critical role for the NAc shell in the transition to chronic pain (7) and the role of the NAc and its connections to the prefrontal cortex in modulating peripheral nociceptive input (6, 8). They are also consistent with recent reports demonstrating that amygdala and hippocampus volume (5) and NAc connectivity to the medial prefrontal cortex (4) can predict the risk of transition to chronic pain.

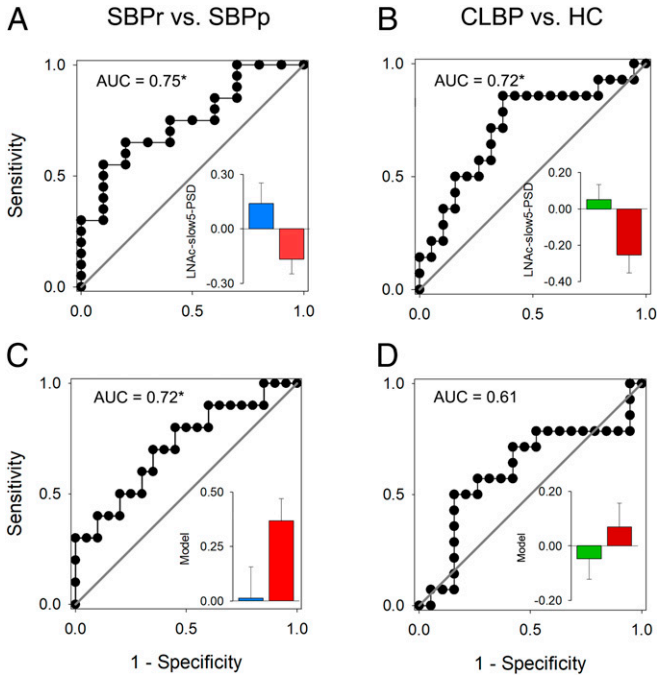

Fig. 4. NAc slow-5 PSD and volume accurately classifies chronic low-back pain patients from an independent dataset collected at a different institution. (*A*) Slow-5 PSD in LNAc accurately classifies 10 SBPr (light blue) and 20 SBPp (red) patients and (*B*) and 14 CLBP (dark red) patients and 19 HCs (green) studied at follow-up in the Chicago study. The PSD in *B* was corrected for age. The *Inset* histogram plot shows the average slow-5 PSD in LNAc within each group. (*C*) and (*D*) Parameters defined in Figs. 1 and 3 were used as features to train an SVM model. We tested our model in an independent dataset not used during model training and collected at a different institution. When used as features in an SVM model, LNAc volume and slow-5 PSD accurately classify SBPp and SBPr patients (*C*). (*D*) The performance of the model did not reach significance when classifying CLBP and HC participants. $*P < 0.05$.

Chronic pain patients suffer from anhedonia and decreased motivation (33, 34). CLBP patients in particular exhibit impaired value-based decision making (35, 36), and disrupted hedonic perception and satiety signals of highly palatable food (37). Studies of animal models of chronic pain have replicated some of these findings (38, 39) and linked reduced motivation to a hypodopaminergic tone in both patients and animal models (40). The NAc is well known to play a central role in hedonic (41) and motivated behavior (11). It contains an abundance of μ-opioid receptors (42), receives mesolimbic dopaminergic projections, and is thought to act as a limbic–motor interface (43) translating motivation into motor action. Midbrain dopaminergic projections to the NAc fire in response to both rewarding and aversive stimuli (44). Brain areas where hedonic and/or incentive value of stimuli are encoded such as orbitofrontal and ventromedial prefrontal cortex (45) and anterior insula (46) send projections to the NAc which in turn projects to the ventral pallidum (47) and lateral hypothalamus (48). This anatomy allows the NAc to access value signals (e.g., hunger, pain) and to send efferent output to the extrapyramidal motor system (47, 49), hence controlling action selection between competing appetitive drives (50–52). Manipulation of the μ-opioid receptor within the NAc alters hedonic reactions to appetitive stimuli (53) and choices of appetitive rewards (54). Alterations in NAc structure, activity, and connectivity in back-pain patients are therefore consistent with the observations of disrupted hedonic and motivated behavior in chronic pain (33). Some NAc alterations (e.g., smaller volume) predate the development of CLBP, suggesting that chronic pain and disruption in motivation (8) and hedonic encoding (37) might share common neural vulnerabilities. Importantly, these structural and functional alterations in the NAc circuitries are independent of depression and anxiety ratings. In fact, major depression is associated with an enlargement of nucleus accumbens volume, which shrinks after successful treatment (55). The opposite findings could henceforth help us untangle the overlapping pathophysiology (56) of chronic pain and major depression.

NAc shell and core play different roles in value-based associative learning (57). The core is thought to mediate cue–outcome association (i.e., similar to the dorsal striatum) and the shell is thought to encode hedonic (positive or negative) value of stimuli (12). While altered NAc structure and connectivity implies generalized changes in motivated behaviors in back-pain patients, altered NAc connectivity, specifically putative shell in at risk back pain (i.e., SBPp), could be associated with disrupted hedonic encoding observed in chronic pain (6, 37, 58). Putative shell also develops loss of PSD within the slow-5 frequency band in SBPp patients at follow-up, whereas both putative shell and core exhibit this change in the CLBP patients. These observations suggest that the NAc shell activity is affected early during pain chronification and are consistent with recent animal studies showing that NAc shell is sufficient to drive peripheral nociception (7) and pain-induced negative affect (59). The altered *δ-fc-NAc* in SBP patients at baseline, on the one hand, and the increased *δ-fc-NAc* to rACC connectivity in SBPp patients at follow-up on the other hand, suggest that NAc connectivity is locally altered during subacute pain processing and spreads to other limbic regions as pain becomes chronic.

Our subacute back-pain patients were recruited if their pain intensity was larger than 20/100 on a VAS scale and the observed average back-pain rating was around 30/100 at baseline. This is a relatively low level of pain compared to clinical pain studies in the literature (4, 60). Nevertheless, back-pain intensity fluctuates on a rather short time scale (minutes) (37, 61) and our patients reported constant back pain more days than not. While we may have included patients suffering from a milder form of low-back pain, our sample of SBP patients had a broad range of pain intensity levels (Fig. 2*D*). In addition, SBPr and SBPp patients had similar levels of pain at baseline.

In conclusion, the NAc functional and structural characteristic are central to the pathophysiology of chronic low-back pain. Loss of PSD within the slow-5 frequency band of NAc activity in particular is a signature (3) of chronic pain that showed significant accuracy in classifying chronic low-back pain patients and is consistent with the new neuroimaging and preclinical literature on the role of NAc persistence of clinical pain (6–8). The measurement of this feature follows standard brain image analysis procedures and is generalizable across scanners and laboratories.

Materials and Methods

Participants.

Data collected at Yale University. The study recruited 40 SBP patients (16 females, average age ± SEM = 31.7 ± 1.7 y), 28 CLBP patients (17 females, 32.2 ± 2.0 y), and 30 HCs (14 females, 31.1 ± 2.0 y). CLBP patients were studied at one time point only. The SBP patients and HCs were followed up longitudinally for a median duration of ∼1 y. All SBP patients reported low-back pain of at least 20/100 on the VAS (0 to 100, where 100 = maximum imaginable pain and 0 = no pain) for the previous 6 to 16 wk with no back pain or pain at other locations in the 12 mo prior to the onset of the current episode. CLBP patients reported low-back pain of at least 30/100 on a VAS for at least 1 y. Participants were excluded if they reported pain at other locations, systemic illnesses, psychiatric diseases, prior traumatic brain injury, or if they tested positive for a controlled substance on a urine toxicology test. All patients reported no or less than mild depression (reported BDI score between 14 and 19) except three CLBP patients who reported moderate depression (BDI <28). (See *SI Appendix*, Tables S1 and S3 for complete

demographic and clinical data.) Data collection took place between July 2014 and April 2019.

Longitudinal Follow-Up. Of the 40 SBP patients, 35 (87.5%) presented for follow-up (32.5 ± 1.9 y, 14 females) and completed questionnaires, 26 (65%) consented to scan, and 5 were lost to follow-up. Of the 30 healthy controls, 16 (53.3%) presented for follow-up (age = 31.6 ± 2.5 y, 7 females) 14 (46.7%) consented to scan, 11 (36.7) were not yet due for follow-up, and 5 (16.7%) were lost to follow-up. The median duration at follow-up was 59.4 wk (*SI Appendix*, Table S3). Consistent with the recommendations of the Initiative on Methods, Measurements and Pain Assessements in Clinical Trials (IMMPACT) (62) SBP patients were dichotomized into recovered back-pain patients (SBPr, $n = 19$) if their back-pain intensity dropped ≥30% on the VAS relative to the pain at entry into the study or into persistent back-pain patients (SBPp, $n = 16$) otherwise. SBP patients who dropped out at follow-up and SBP patients who completed the follow-up visit did not differ on rated back-pain intensity at entry into the study (dropped out = 3.4 ± 1.0, completed = 3.1 ± 0.3, $P = 0.72$ on the VAS), or pain duration in weeks (dropped out = 8.5 ± 3.6, completed = 9.5 ± 0.7 wk; $P = 0.64$). This study was approved by the Yale University Institutional Review Board. All participants gave informed consent for inclusion in our study.

Data Made Available Online. To validate our findings in an independent dataset, we obtained datasets collected at different sites. Data were obtained from the OpenPain Project (OPP) database (http://www.openpain.org). The OPP Project (principal investigator: A. Vania Apkarian, PhD at Northwestern University) is supported by the National Institute of Neurological Disorders and Stroke (NINDS) and National Institute of Drug Abuse (NIDA). Therefore, we analyzed three additional resting-state fMRI datasets. The first dataset was collected in Chicago at Northwestern University and included 24 CLBP patients (11 females, 49.5 ± 2.0 y) and 30 healthy controls (13 females, 48.5 ± 1.7 y). The second dataset was also collected in Chicago at Northwestern University, part of a longitudinal study using fMRI to study the transition from subacute to CLBP (4, 5). These data included participants studied during the follow-up visit: 14 CLBP patients (6 females, 46.9 ± 1.9 y), 19 healthy controls (8 females, 37.5 ± 1.6 y), and 30 SBP patients (15 females, 45.6 ± 1.8 y). The third dataset (63) was collected at Cambridge University and included 20 CLBP patients (12 females, 46.7 ± 2.6 y) and 38 healthy controls (14 females, 38.9 ± 2.2 y). Both datasets are freely available at http://www.openpain.org/.

Pain Characteristics, Mood, and Affect. Patients reported their pain using the sfMPQ (64), the NPS (65), and the PCS (66) at all visits. They reported their mood and anxiety levels using the Beck's Depression and the Beck's Anxiety Inventories (67, 68).

Scanning Parameters. Participants underwent an anatomical T1-weighted scan, and two consecutive 6-min-long resting-state scans. Siemens 3.0 T Trio B magnet equipped with a 32-channel head coil was used to acquire the images. MPRAGE 3D T1-weighted acquisition sequence was as follows: TR/TE = 1,900/2.52 ms, flip angle = 9°, matrix 256 × 256 with 176 slices (1 mm thick) acquired in the same orientation as the functional data. During the functional scans, participants were asked to stare at a crosshair; the functional acquisition sequence was as follows: TR/TE = 1,000/30.0 ms, flip angle = 60°, matrix 110 × 110 × 60 with 2 × 2 × 2 mm voxels, and an acceleration factor of 4.

Volume Calculations. Structural data were analyzed with the standard automated processing stream of the Functional Magnetic Resonance Imaging of the Brain (FMRIB) software library (FSL) 5.0.10 that shows high reliability across laboratories (69). The analysis sequence includes skull extraction, a two-stage linear subcortical registration, and segmentation using the Integrated Registration and Segmentation Tool (FIRST) (70), part of FMRIB. The volumes of right and left nucleus accumbens (NAc), amygdala, hippocampus, and thalamus were calculated for each participant and normalized to standard MNI space. The normalization coefficient was calculated using FSL SIENAX (71). Quality control included: 1) visual inspection of subcortical segmentation to identify gross mismatches between underlying anatomy and FIRST output; 2) identification and exclusion of outliers defined using Tukey's method (72); and 3) comparison of SNR within each subcortical structure across groups. SNR was calculated as the mean signal within a certain structure minus the mean signal outside the brain divided by the SD of the signal outside the brain. Outliers were defined independently for each structure. Three participants' data were excluded as such. Importantly, removing these individuals did not change our statistical results.

Subcortical volume calculations were repeated using the standard automated cortical and subcortical segmentations by FreeSurfer 5.0 (http://surfer.nmr.mgh.harvard.edu/) to check volume reproducibility of the results across different segmentation algorithms. FreeSurfer's analysis sequence includes motion correction, removal of the skull using watershed/surface deformation procedure, normalization in Talairach space, and segmentation of the brain structures based on the existing atlas containing probabilistic information on the location of the structures (10).

Functional MRI Preprocessing. Two 6-min-long resting-state scans were acquired consecutively while participants stared at a crosshair. The preprocessing of each participant's fMRI time series was performed using the FMRIB Expert Analysis Tool (FEAT). The sequence was published previously by our group (73) and included skull extraction using the Brain Extraction Tool, head motion correction (74), band pass filtering (0.008 to 0.2 Hz), and spatial smoothing (5-mm full width at half maximum Gaussian blur). Several sources of spurious variance were removed from the data with linear regression. The six parameters obtained by rigid head motion correction along with their temporal derivative, and 10 components derived from noise ROIs were regressed out from the data. The latter components were identified following an anatomical approach as described in ref. 75. Briefly, cerebrospinal fluid (CSF) and white matter time series were extracted from each subject's fMRI data based on masks derived from the high-resolution anatomical image using FSL FAST (76). Next, principal component analysis was applied to obtain the first five white matter and first five CSF components. After preprocessing, functional scans were registered into the MNI space. Registration to high-resolution structural and/or MNI images was carried out using FLIRT (74, 77). Registration from high-resolution structural to MNI space was then further refined using FNIRT nonlinear registration (78).

Seed-Based Analysis. Seed-based connectivity was determined following a well-defined method (79) and used previously by our group (73). To investigate whether brain networks correlated with specific regional activity (seed) as a function of group, seeds were defined from a probabilistic parcellation of putative nucleus accumbens shell and core (16, 17) (see *Results*). Average BOLD time course of all voxels within the ROIs was extracted and then the correlation coefficient between this time course and the time variability of all brain voxels were computed using Matlab. Head motion can cause spurious but spatially structured changes in functional correlations (80). To minimize these effects, all subjects were movement scrubbed (80). This procedure uses temporal masks to remove motion-contaminated data from regression and correlation calculations by excising unwanted data. Frames in which collective displacement (FD) across all six rigid body movement correction parameters exceeded FD >0.5 mm (assuming 50-mm cortical sphere radius) were identified. We excluded frames flagged by this criterion. Runs with >40% frames flagged were omitted from analyses. Correlation coefficients were converted to a normal distribution using the Fisher z transform. These values were then converted to z scores (i.e., normalized correlation values) by dividing by the square root of the variance, estimated as $1/\sqrt{df-3}$, where df represents the degrees of freedom in our measurements (i.e., the number of volumes acquired). Because the BOLD time courses of consecutive samples are not statistically independent, the degrees of freedom were corrected by a factor according to Bartlet theory (81). Group differences in seed-based connectivity were identified using permutation-based inference (82) to allow rigorous comparisons of significance within the framework of the general linear model with $P < 0.05$. Group differences were tested against 10,000 random permutations, which inherently accounts for multiple comparisons, using the Randomize part of FSL (83). Group contrast clusters were identified using the threshold-free cluster enhancement (TFCE) method (84), which bypasses the arbitrary threshold necessary in methods that use voxel-based thresholds. To test for the effects of time (baseline vs. follow-up) on functional connectivity, we used a repeated measure (baseline vs. follow-up) by groups (HC vs. SBPp vs. SBPr) ANCOVA. We first generated a subject-specific template for each participant using their baseline and follow-up anatomical scans to account for possible longitudinal changes in anatomy. The template was generated using FreeSurfer's command "mri_robust_template." Next, functional connectivity maps from baseline and follow-up were registered to this template which in turn was registered to the MNI space. Finally, the within-subject GLM analysis was run to test for time effects using 10,000 permutations (randomize, FSL).

Spectral Analysis. Spectral analysis was performed using custom Matlab (The MathWorks, 2010) routines and is similar to methods reported previously (21). Frequency power of the BOLD signal was determined voxelwise using

Welch's method and normalized by dividing by total power. This normalization was necessary as the absolute power of BOLD remains unknown simply because the absolute intensity of BOLD signal in time space is also unknown and assigned an arbitrary value in all standard fMRI analyses. The average power of each frequency band (30) slow-5 (0.01 to 0.027 Hz), slow-4 (0.027 to 0.073 Hz), slow-3 (0.073 to 0.198 Hz), and slow-2 (0.198 to 0.5 Hz) was calculated at each voxel and converted into four different maps for each subject. Individual subject maps were transformed into standard space as described in the preprocessing section and multiplied by a standard gray matter mask. Subject-level maps were transformed to *z*-score maps by subtracting the mean voxelwise power for the entire brain and dividing by the SD. Group differences were generated using a similar nonparametric permutation and thresholding approaches described under seed-based analysis.

Support Vector Machine Learning and Model Building. We used the slow-5 power spectral density and nucleus accumbens volume of each hemisphere separately as features in a SVM (85) learning analysis to classify subjects: SBPp vs. SBPr patients or CLBP patients vs. HCs. We trained and tested the SVM model on independent datasets collected at different institutions. Features were selected and their weights were learned without using information from the test set. For validation, the trained models were used to predict outcomes in the test set. For models combining more than one measure, we learned the relative weights of each measure using a linear SVM. Free hyperparameters were first chosen from a grid of proposed values using cross-validation within the training set (86), and then models were fit to the full training dataset using the optimal hyperparameters. Finally, models were tested on an independent dataset. We trained our model on data collected at Yale University (described above) and on data available online at http://www.openpain.org/ from Cambridge University (63). The test datasets (*SI Appendix*, Table S6) were not used in any of our previous analyses or during the training of the SVM model. We first harmonized data from different scanners using the Combat method (87, 88). Next, we trained a linear SVM to discriminate between HC and CBP subjects in the training datasets pooled together and evaluated the discriminative power of the distance to the decision hyperplane in two sets of subjects from the Chicago longitudinal cohort visit 4 (HC vs. CLBP, and SBPr vs. SBPp patients) as quantified by the area under the receiver operating characteristic (ROC) curve (AUC). Significance of the result was established by random permutation of the validation set labels (10^3 permutations). We used the LinearSVC implementation in *scikit-learn* (89) with default parameters with the following exceptions: "loss" parameter was set to "hinge," "class_weight" was set to "balanced," and "C" was chosen by internal cross validation (grid search, 5 internal cross-validation folds) from 8 possible values ranging between 10^{-5} and 10^3 equally spaced in logarithmic units. The code is freely available at this link: ftp://openpain.org/AccumbensChronicPainSignature. In imbalanced test datasets, both classes were given equal weights because the AUC depends only on the fraction of errors in one class, and the fraction of hits in the other class as the decision threshold is changed. The fraction of labels for each class remained fixed during permutation testing, ensuring that significant results could not be explained by the distribution of labels in the test set.

Statistical Analyses. Statistical analyses of demographic and clinical variables and of extracted subcortical volumes were performed using Statistica Software (TIBCO, Inc.). Between-group analysis was performed using general linear model or ANOVA. All analyses of subcortical volumes accounted for age, sex, and intracranial volumes. We used linear regression analyses to investigate the relationships between reported pain on the VAS and brain measures.

Data Availability. All data presented in this study are freely available at ftp://openpain.org/AccumbensChronicPainSignature (90).

ACKNOWLEDGMENTS. This work was supported by funds from the National Institute on Drug Abuse (NIDA: 5K08DA037525) and from the Psychiatry Department at the Yale School of Medicine.

1. E. L. Hurwitz, K. Randhawa, H. Yu, P. Côté, S. Haldeman, The global spine care initiative: A summary of the global burden of low back and neck pain studies. *Eur. Spine J.* **27** (suppl. 6), 796–801 (2018).
2. Anonymous, *Relieving Pain in America: A Blueprint for Transforming Prevention, Care, Education, and Research* (Institute of Medicine of the National Academies, Washington, DC, 2011).
3. C. W. Woo, T. D. Wager, Neuroimaging-based biomarker discovery and validation. *Pain* **156**, 1379–1381 (2015).
4. M. N. Baliki *et al*., Corticostriatal functional connectivity predicts transition to chronic back pain. *Nat. Neurosci.* **15**, 1117–1119 (2012).
5. E. Vachon-Presseau *et al*., Corticolimbic anatomical characteristics predetermine risk for chronic pain. *Brain* **139**, 1958–1970 (2016).
6. M. Lee *et al*., Activation of corticostriatal circuitry relieves chronic neuropathic pain. *J. Neurosci.* **35**, 5247–5259 (2015).
7. W. Ren *et al*., The indirect pathway of the nucleus accumbens shell amplifies neuropathic pain. *Nat. Neurosci.* **19**, 220–222 (2016).
8. N. Schwartz *et al*., Chronic pain. Decreased motivation during chronic pain requires long-term depression in the nucleus accumbens. *Science* **345**, 535–542 (2014).
9. A. V. Apkarian *et al*., Role of adult hippocampal neurogenesis in persistent pain. *Pain* **157**, 418–428 (2016).
10. B. Fischl, FreeSurfer. *Neuroimage* **62**, 774–781 (2012).
11. S. Ikemoto, Dopamine reward circuitry: Two projection systems from the ventral midbrain to the nucleus accumbens-olfactory tubercle complex. *Brain Res. Brain Res. Rev.* **56**, 27–78 (2007).
12. E. A. West, R. M. Carelli, Nucleus accumbens core and shell differentially encode reward-associated cues after reinforcer devaluation. *J. Neurosci.* **36**, 1128–1139 (2016).
13. E. Navratilova *et al*., Pain relief produces negative reinforcement through activation of mesolimbic reward-valuation circuitry. *Proc. Natl. Acad. Sci. U.S.A.* **109**, 20709–20713 (2012).
14. I. K. Martikainen *et al*., Chronic back pain is associated with alterations in dopamine neurotransmission in the ventral striatum. *J. Neurosci.* **35**, 9957–9965 (2015).
15. C. W. Woo *et al*., Quantifying cerebral contributions to pain beyond nociception. *Nat. Commun.* **8**, 14211 (2017).
16. M. N. Baliki *et al*., Parceling human accumbens into putative core and shell dissociates encoding of values for reward and pain. *J. Neurosci.* **33**, 16383–16393 (2013).
17. X. Xia *et al*., Multimodal connectivity-based parcellation reveals a shell-core dichotomy of the human nucleus accumbens. *Hum. Brain Mapp.* **38**, 3878–3898 (2017).
18. F. Ambroggi, A. Ghazizadeh, S. M. Nicola, H. L. Fields, Roles of nucleus accumbens core and shell in incentive-cue responding and behavioral inhibition. *J. Neurosci.* **31**, 6820–6830 (2011).
19. J. H. Steiger, Tests for comparing elements of a correlation matrix. *Psychol. Bull.* **87**, 245–251 (1980).
20. E. P. Duff *et al*., The power of spectral density analysis for mapping endogenous BOLD signal fluctuations. *Hum. Brain Mapp.* **29**, 778–790 (2008).
21. X. N. Zuo *et al*., The oscillating brain: Complex and reliable. *Neuroimage* **49**, 1432–1445 (2010).
22. J. Y. Kim *et al*., Increased power spectral density in resting-state pain-related brain networks in fibromyalgia. *Pain* **154**, 1792–1797 (2013).
23. M. N. Baliki, A. T. Baria, A. V. Apkarian, The cortical rhythms of chronic back pain. *J. Neurosci.* **31**, 13981–13990 (2011).
24. S. Malinen *et al*., Aberrant temporal and spatial brain activity during rest in patients with chronic pain. *Proc. Natl. Acad. Sci. U.S.A.* **107**, 6493–6497 (2010).
25. Z. Q. Zhang *et al*., [Application of amplitude of low-frequency fluctuation to the temporal lobe epilepsy with bilateral hippocampal sclerosis: An fMRI study]. *Zhonghua Yi Xue Za Zhi* **88**, 1594–1598 (2008).
26. F. Zhou, L. Wu, L. Guo, Y. Zhang, X. Zeng, Local connectivity of the resting brain connectome in patients with low back-related leg pain: A multiscale frequency-related Kendall's coefficient of concordance and coherence-regional homogeneity study. *Neuroimage Clin.* **21**, 101661 (2019).
27. F. Zhou *et al*., Compressing the lumbar nerve root changes the frequency-associated cerebral amplitude of fluctuations in patients with low back/leg pain. *Sci. Rep.* **9**, 2246 (2019).
28. F. Zhou *et al*., Altered low-frequency oscillation amplitude of resting state-fMRI in patients with discogenic low-back and leg pain. *J. Pain Res.* **11**, 165–176 (2018).
29. D. J. Hodkinson *et al*., Increased amplitude of thalamocortical low-frequency oscillations in patients with migraine. *J. Neurosci.* **36**, 8026–8036 (2016).
30. S. R. Gohel, B. B. Biswal, Functional integration between brain regions at rest occurs in multiple-frequency bands. *Brain Connect.* **5**, 23–34 (2015).
31. G. Buzsáki, A. Draguhn, Neuronal oscillations in cortical networks. *Science* **304**, 1926–1929 (2004).
32. D. M. Green, J. A. Swets, *Signal Detection Theory and Psychophysics* (Wiley, New York, 1966), p. xi, 455 pp.
33. D. C. Turk, J. Audette, R. M. Levy, S. C. Mackey, S. Stanos, Assessment and treatment of psychosocial comorbidities in patients with neuropathic pain. *Mayo Clin. Proc.* **85** (suppl. 3), S42–S50 (2010).
34. E. L. Garland, M. Trøstheim, M. Eikemo, G. Ernst, S. Leknes, Anhedonia in chronic pain and prescription opioid misuse. *Psychol. Med.*, 1–12 (2019).
35. A. V. Apkarian *et al*., Chronic pain patients are impaired on an emotional decision-making task. *Pain* **108**, 129–136 (2004).
36. S. Tamburin *et al*., Cognition and emotional decision-making in chronic low back pain: An ERPs study during Iowa gambling task. *Front. Psychol.* **5**, 1350 (2014).
37. P. Geha, I. Dearaujo, B. Green, D. M. Small, Decreased food pleasure and disrupted satiety signals in chronic low back pain. *Pain* **155**, 712–722 (2014).
38. M. Pais-Vieira, M. M. Mendes-Pinto, D. Lima, V. Galhardo, Cognitive impairment of prefrontal-dependent decision-making in rats after the onset of chronic pain. *Neuroscience* **161**, 671–679 (2009).

39. G. Ji *et al*., Cognitive impairment in pain through amygdala-driven prefrontal cortical deactivation. *J. Neurosci.* **30**, 5451–5464 (2010).
40. A. M. Taylor, S. Becker, P. Schweinhardt, C. Cahill, Mesolimbic dopamine signaling in acute and chronic pain: Implications for motivation, analgesia, and addiction. *Pain* **157**, 1194–1198 (2016).
41. S. Peciña, K. S. Smith, K. C. Berridge, Hedonic hot spots in the brain. *Neuroscientist* **12**, 500–511 (2006).
42. A. L. Jongen-Rělo, H. J. Groenewegen, P. Voorn, Evidence for a multi-compartmental histochemical organization of the nucleus accumbens in the rat. *J. Comp. Neurol.* **337**, 267–276 (1993).
43. G. J. Mogenson, D. L. Jones, C. Y. Yim, From motivation to action: Functional interface between the limbic system and the motor system. *Prog. Neurobiol.* **14**, 69–97 (1980).
44. F. Porreca, E. Navratilova, Reward, motivation, and emotion of pain and its relief. *Pain* **158** (suppl. 1), S43–S49 (2017).
45. S. N. Haber, B. Knutson, The reward circuit: Linking primate anatomy and human imaging. *Neuropsychopharmacology* **35**, 4–26 (2010).
46. M. Chikama, N. R. McFarland, D. G. Amaral, S. N. Haber, Insular cortical projections to functional regions of the striatum correlate with cortical cytoarchitectonic organization in the primate. *J. Neurosci.* **17**, 9686–9705 (1997).
47. H. J. Groenewegen, C. I. Wright, A. V. Beijer, P. Voorn, Convergence and segregation of ventral striatal inputs and outputs. *Ann. N. Y. Acad. Sci.* **877**, 49–63 (1999).
48. S. N. Haber, E. Lynd, C. Klein, H. J. Groenewegen, Topographic organization of the ventral striatal efferent projections in the rhesus monkey: An anterograde tracing study. *J. Comp. Neurol.* **293**, 282–298 (1990).
49. H. J. Groenewegen, C. I. Wright, A. V. Beijer, The nucleus accumbens: Gateway for limbic structures to reach the motor system? *Prog. Brain Res.* **107**, 485–511 (1996).
50. M. R. Roesch, T. Singh, P. L. Brown, S. E. Mullins, G. Schoenbaum, Ventral striatal neurons encode the value of the chosen action in rats deciding between differently delayed or sized rewards. *J. Neurosci.* **29**, 13365–13376 (2009).
51. J. J. Day, J. L. Jones, R. M. Carelli, Nucleus accumbens neurons encode predicted and ongoing reward costs in rats. *Eur. J. Neurosci.* **33**, 308–321 (2011).
52. S. B. Floresco, The nucleus accumbens: An interface between cognition, emotion, and action. *Annu. Rev. Psychol.* **66**, 25–52 (2015).
53. A. E. Kelley *et al*., Opioid modulation of taste hedonics within the ventral striatum. *Physiol. Behav.* **76**, 365–377 (2002).
54. M. Zhang, B. A. Gosnell, A. E. Kelley, Intake of high-fat food is selectively enhanced by mu opioid receptor stimulation within the nucleus accumbens. *J. Pharmacol. Exp. Ther.* **285**, 908–914 (1998).
55. C. G. Abdallah *et al*., The nucleus accumbens and ketamine treatment in major depressive disorder. *Neuropsychopharmacology* **42**, 1739–1746 (2017).
56. C. G. Abdallah, P. Geha, Chronic pain and chronic stress: Two sides of the same coin? *Chronic Stress (Thousand Oaks)* **1**, 1–10 (2017).
57. F. Mannella, K. Gurney, G. Baldassarre, The nucleus accumbens as a nexus between values and goals in goal-directed behavior: A review and a new hypothesis. *Front. Behav. Neurosci.* **7**, 135 (2013).
58. S. J. Thompson *et al*., Chronic neuropathic pain reduces opioid receptor availability with associated anhedonia in rat. *Pain* **159**, 1856–1866 (2018).
59. N. Massaly *et al*., Pain-induced negative affect is mediated via recruitment of the nucleus accumbens Kappa opioid system. *Neuron* **102**, 564–573.e6 (2019).
60. J. S. Gewandter *et al*., Research design considerations for chronic pain prevention clinical trials: IMMPACT recommendations. *Pain* **156**, 1184–1197 (2015).
61. J. M. Foss, A. V. Apkarian, D. R. Chialvo, Dynamics of pain: Fractal dimension of temporal variability of spontaneous pain differentiates between pain States. *J. Neurophysiol.* **95**, 730–736 (2006).
62. R. H. Dworkin *et al*.; IMMPACT, Core outcome measures for chronic pain clinical trials: IMMPACT recommendations. *Pain* **113**, 9–19 (2005).
63. H. Mano *et al*., Classification and characterisation of brain network changes in chronic back pain: A multicenter study. *Wellcome Open Res.* **3**, 19 (2018).
64. R. Melzack, The short-form McGill pain questionnaire. *Pain* **30**, 191–197 (1987).
65. B. S. Galer, M. P. Jensen, Development and preliminary validation of a pain measure specific to neuropathic pain: The neuropathic pain scale. *Neurology* **48**, 332–338 (1997).
66. M. Sullivan, S. Bishop, J. Pivik, The pain catastrophizing scale: Development and validation. *Psychol. Assess.* **7**, 524–532 (1995).
67. A. Beck, R. Steer, *Manual for the Beck Anxiety Inventory* (Psychological Corporation, San Antonio, 1993).
68. A. Beck, R. Steer, *Beck Depression Inventory* (Psychological Corporation, San Antonio, 1993).
69. A. C. Nugent *et al*., Automated subcortical segmentation using FIRST: Test-retest reliability, interscanner reliability, and comparison to manual segmentation. *Hum. Brain Mapp.* **34**, 2313–2329 (2013).
70. B. Patenaude, S. M. Smith, D. N. Kennedy, M. Jenkinson, A Bayesian model of shape and appearance for subcortical brain segmentation. *Neuroimage* **56**, 907–922 (2011).
71. S. M. Smith *et al*., Accurate, robust, and automated longitudinal and cross-sectional brain change analysis. *Neuroimage* **17**, 479–489 (2002).
72. J. W. Tukey, *Exploratory Data Analysis* (Addison-Wesley Series in Behavioral Science, Addison-Wesley Pub. Co., Reading, MA, 1977), p. xvi, 688 p.
73. P. Geha, G. Cecchi, R. Todd Constable, C. Abdallah, D. M. Small, Reorganization of brain connectivity in obesity. *Hum. Brain Mapp.* **38**, 1403–1420 (2017).
74. M. Jenkinson, P. Bannister, M. Brady, S. Smith, Improved optimization for the robust and accurate linear registration and motion correction of brain images. *Neuroimage* **17**, 825–841 (2002).
75. Y. Behzadi, K. Restom, J. Liau, T. T. Liu, A component based noise correction method (CompCor) for BOLD and perfusion based fMRI. *Neuroimage* **37**, 90–101 (2007).
76. Y. Zhang, M. Brady, S. Smith, Segmentation of brain MR images through a hidden Markov random field model and the expectation-maximization algorithm. *IEEE Trans. Med. Imaging* **20**, 45–57 (2001).
77. M. Jenkinson, S. Smith, A global optimisation method for robust affine registration of brain images. *Med. Image Anal.* **5**, 143–156 (2001).
78. M. Jenkinson, C. F. Beckman, T. E. Behrens, M. M. Woolrich, S. M. Smith, FSL. *Neuroimage* **62**, 782–790 (2012).
79. M. D. Fox *et al*., The human brain is intrinsically organized into dynamic, anticorrelated functional networks. *Proc. Natl. Acad. Sci. U.S.A.* **102**, 9673–9678 (2005).
80. J. D. Power, K. A. Barnes, A. Z. Snyder, B. L. Schlaggar, S. E. Petersen, Spurious but systematic correlations in functional connectivity MRI networks arise from subject motion. *Neuroimage* **59**, 2142–2154 (2012).
81. G. M. Jenkins, D. G. Watts, *Spectral Analysis and its Applications* (Holden-Day Series in Time Series Analysis, Holden-Day, San Francisco, 1968), p. xviii, 525 p.
82. T. E. Nichols, A. P. Holmes, Nonparametric permutation tests for functional neuroimaging: A primer with examples. *Hum. Brain Mapp.* **15**, 1–25 (2002).
83. A. M. Winkler, G. R. Ridgway, M. A. Webster, S. M. Smith, T. E. Nichols, Permutation inference for the general linear model. *Neuroimage* **92**, 381–397 (2014).
84. S. M. Smith, T. E. Nichols, Threshold-free cluster enhancement: Addressing problems of smoothing, threshold dependence and localisation in cluster inference. *Neuroimage* **44**, 83–98 (2009).
85. C. Cortes, V. Vapnik, Support-vector networks. *Mach. Learn.* **20**, 273–297 (1995).
86. S. Varma, R. Simon, Bias in error estimation when using cross-validation for model selection. *BMC Bioinformatics* **7**, 91 (2006).
87. J. P. Fortin *et al*., Harmonization of cortical thickness measurements across scanners and sites. *Neuroimage* **167**, 104–120 (2018).
88. W. E. Johnson, C. Li, A. Rabinovic, Adjusting batch effects in microarray expression data using empirical Bayes methods. *Biostatistics* **8**, 118–127 (2007).
89. F. Pedregosa *et al*., Scikit-learn: Machine learning in Python. *J. Mach. Learn. Res.* **12**, 2825–2830 (2011).
90. M. M. Makary *et al*., AccumbensChronicPainSignature. OpenPain. ftp://openpain.org/AccumbensChronicPainSignature. Deposited 26 March 2020.